

# Texture-adaptive active contour models

Thomas Lehmann, Jörg Bredno, and Klaus Spitzer  
Institute of Medical Informatics,  
Aachen University of Technology (RWTH),  
D-52057 Aachen, Germany

## Abstract

Unsupervised segmentation is a key challenge for automated quantification of medical images. Although a balloon model is able to detect arbitrarily shaped objects in images, it requires careful adjustment of parameters prior to segmentation.

Based on global texture analyses, our method allows to set these parameters automatically for heterogeneous images such as MRI, ultrasound, or microscopy. Cooccurrence matrices are extracted from prototype images and used as feature vectors to train a synergetic classifier. These matrices are computed likewise for all other images. To control segmentation, similarity measures for these features are applied to weight the linear combination of the prototype parameters.

The method was tested on 81 synthetic images and applied to a set of 1616 heterogeneous radiographs. Setting the parameters of active contour models by the proposed method improves the acceptance rate of unsupervised segmentation from 31% up to 71%.

**Keywords:** unsupervised segmentation, active contours, balloon model, parameterization, texture analysis

## 1 Introduction

In medical imaging, quantitative analyses require segmentation to identify objects of interest [1]. Since manual segmentation is tedious, automatic or semi-automatic segmentation methods have been examined [2]. Unsupervised segmentation of images is a key challenge for any automated analysis of images and major goal of research in bio-medical image processing.

So far, systems for automated quantification rely on reproducibly acquired images with similar appearance of considered objects. However, in medical imaging this assumption often is violated. Normalization and fixed units for image values are obtained from computed tomography but neither from magnetic resonance, ultrasound, radiographic, nor microscopic imaging. Furthermore, biological tissue often drastically varies in material properties the imaging is based on (e.g. radiometric density or sonographic reflection coefficients). Hence, the

appearance of medical images is not constant even if images are captured by identical devices.

When carefully adapted, active contours have been shown to result in reliable segmentation [2,3,4]. However, the adjustment of parameters is required for each task or application and still performed manually by technical experts. In our approach, the parameter adjustment is done automatically. Different sets of parameters are handled by texture-adaptive categorization of images.

Following a brief introduction to the balloon model that is used for segmentation (Sec. 2.1), we describe the training phase of a synergetic classifier for texture discrimination (Sec. 2.2) and the adaptive parameterization for individual images using this classifier (Sec. 2.3). In Section 2.4, our method is generalized to color images. The classification that is based on the logarithm of cooccurrence matrices is evaluated in Section 3.1. Results are presented for a synthetic images (Sec. 3.2) as well as a heterogeneous archive of radiographs (Sec. 3.3).

## 2 Method

Our method combines a robust and well-known balloon model with an a-priori texture analysis that is used to determine the similarity of the current image with trained images. This allows to adapt the parameterization of the segmentation procedure.

### 2.1 Balloon model for segmentation

For segmentation of medical images, we apply a generalized balloon model [3] that is based on finite element meshes [4]. The edge elements of simplex meshes move under mechanical influences until they contact significant borders of objects in the

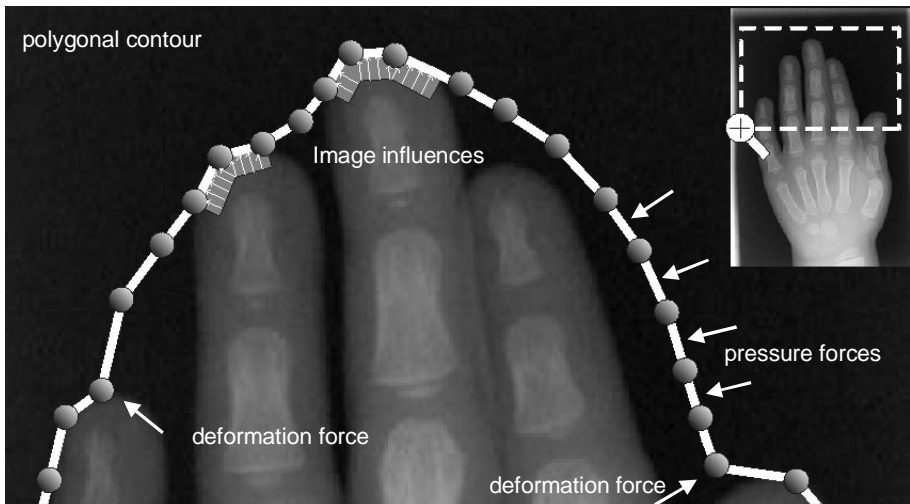


Figure 1: Influences acting on the balloon during iterative segmentation of a radiograph.

image. The edges of a polygon are moved iteratively by forces resulting from the pressure of the balloon, a deformation force that is reducing the 2nd order derivative of the polygons, and image influences (Fig. 1). The gray or color values are interpreted as image potentials resulting in region-based external forces and give local resistance to the movement of edges (Fig. 2).

Based on this model, the algorithm locates arbitrarily shaped structures in images without any initial contour. In comparison to classic snake approaches and all their variations [5], the balloon-based algorithm requires more careful consideration of the parameters controlling the segmentation. For our model, the following influences for the finite elements have to be adjusted according to the image:

- The maximal and minimal length of edges of the polygonal contour.
- The scale of gradients in the image occurring at the border or relevant objects.
- The appearance and intensity of these gradients, which are coded in the potentials of image values.
- The strength of the deformation force.
- The strength of the pressure force.

A unique set of segmentation parameters can be used for all images with similar appearance of objects of interest [6]. To enable automatic segmentation of arbitrary images, a training phase is needed prior to segmentation.

## 2.2 Training of texture

For unsupervised segmentation of heterogeneous image sets, the parameters have to be adjusted without a-priori knowledge on image contents. Therefore, global texture statistics are used to determine the similarity of appearances between



Figure 2: Visualization of image potentials for the radiograph in Figure 1.

images. In a training phase, we browse a representative subset of images to identify significant differences in appearance. For each class of appearance, a prototype image is chosen arbitrarily. The parameters for this prototype image are set using an automated method that employs an exemplary manual segmentation. Therefore, this initialization can be done easily by physicians [6]. Then, the appearance of those prototypes is described by their cooccurrence-matrix [7]. Such texture statistics are frequently used for texture classification [8,9].

All prototypes are downscaled to 256x256 pixels and the gray-scale is reduced to 64 using nearest-neighbor interpolation [10]. Cooccurrence matrices are extracted for these images with a displacement of 5. The segmentation parameters must be adjusted such that the balloon model is allowed to overcome irrelevant structures in the image but stops at the border of considered objects, where notable changes in the appearance of tissues occur. Therefore, the interesting entries in the cooccurrence matrix lay with distance to the main diagonal. Even for large displacements, the entries along the main diagonal significantly are larger than all others. Hence, mathematical operations that compute discriminative measures for these matrices face the danger of numerical instability. Therefore, the logarithm is applied to all entries of the cooccurrence matrix (Fig. 3). The resulting matrix is regarded as a high-dimensional feature vector  $\vec{c}$  and normalized to mean zero and length one. For these features, we use the synergetic classifier proposed in [11] to achieve robust similarity measures.

This classifier relies on an orthonormal basis of adjoint vectors  $\vec{c}_j^+$  for the prototype features  $\vec{c}_i$ . We demand

$$\vec{c}_i \cdot \vec{c}_j^+ = \delta_{ij} \quad (1)$$

for all prototype feature vectors, where  $\delta$  denotes the Kronecker delta symbol with  $\delta_{ij} = 1 \forall i = j, 0$  else. The adjoint cooccurrence features  $\vec{c}_j^+$  are build as a linear

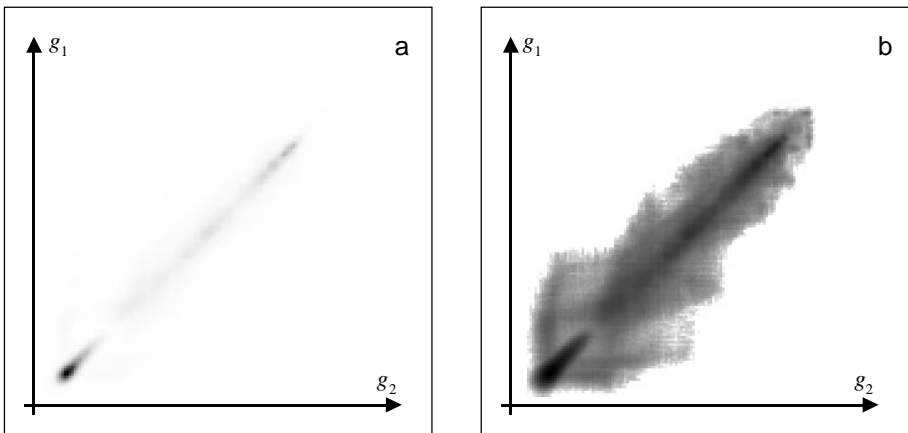


Figure 3: The cooccurrence matrix for gray values  $g_1$  and  $g_2$  of a radiograph are displayed without and with the logarithm of all values, (a) and (b), respectively. The histograms of both images have been stretched individually for contrast enhancement.

combination of all  $n$  prototype features  $\bar{c}_k$ :

$$\bar{c}_j^+ = \sum_{k=1}^n a_{jk} \bar{c}_k \quad (2)$$

Multiplying (2) with the prototype vectors  $\bar{c}_i$  and using (1) for the left side, we obtain a system of  $n^2$  linear equations

$$I = \begin{pmatrix} 1 & \bar{c}_1 \cdot \bar{c}_2 & \cdots & \bar{c}_1 \cdot \bar{c}_n \\ \bar{c}_2 \cdot \bar{c}_1 & 1 & & \bar{c}_2 \cdot \bar{c}_n \\ \vdots & & \ddots & \vdots \\ \bar{c}_n \cdot \bar{c}_1 & \bar{c}_n \cdot \bar{c}_2 & \cdots & 1 \end{pmatrix} \cdot \begin{pmatrix} a_{11} & a_{12} & \cdots & a_{1n} \\ a_{21} & a_{22} & & a_{2n} \\ \vdots & & \ddots & \vdots \\ a_{n1} & a_{n2} & \cdots & a_{nn} \end{pmatrix} \quad (3)$$

with  $I$  denoting the identity matrix. The  $a_{jk}$  can be calculated by inverting the matrix of the scalar products of all prototype feature vectors

$$\begin{pmatrix} a_{11} & a_{12} & \cdots & a_{1n} \\ a_{21} & a_{22} & & a_{2n} \\ \vdots & & \ddots & \vdots \\ a_{n1} & a_{n2} & \cdots & a_{nn} \end{pmatrix} = \begin{pmatrix} 1 & \bar{c}_1 \cdot \bar{c}_2 & \cdots & \bar{c}_1 \cdot \bar{c}_n \\ \bar{c}_2 \cdot \bar{c}_1 & 1 & & \bar{c}_2 \cdot \bar{c}_n \\ \vdots & & \ddots & \vdots \\ \bar{c}_n \cdot \bar{c}_1 & \bar{c}_n \cdot \bar{c}_2 & \cdots & 1 \end{pmatrix}^{-1} \quad (4)$$

They are used to compute the adjoint prototype vectors  $\bar{c}_j^+$  in (2).

### 2.3 Texture-adaptive parameterization

The parameter sets for prototype images resulting from training as well as the adjoint cooccurrence feature vectors  $\bar{c}_j^+$  are used for the segmentation of heterogeneous images.

During segmentation, a cooccurrence feature vector is computed for each image. The scalar products of this vector with the adjoint vectors of all prototypes represent similarities. Therefore, these scalar products are used to automatically create an individual set of parameters for the image.

Let  $\bar{c}_{\text{image}}$  denote the cooccurrence matrix of an image that has to be segmented and  $\bar{P}_j$  be a vector containing the parameters that are used for the segmentation of prototype image  $j$ . Then, the required parameters  $\bar{P}_{\text{image}}$  are calculated from the similarity of the cooccurrence feature  $\bar{c}_{\text{image}}$  and the adjoint prototype features  $\bar{c}_j^+$

$$\bar{P}_{\text{image}} = \frac{\sum_{j=1}^n w_j \bar{P}_j}{\sum_{j=1}^n w_j} \quad \text{with} \quad w_j = \begin{cases} \bar{c}_{\text{image}} \cdot \bar{c}_j^+ & \forall \quad 0 \leq \bar{c}_{\text{image}} \cdot \bar{c}_j^+ \leq 1 \\ 1 - \bar{c}_{\text{image}} \cdot \bar{c}_j^+ & \forall \quad 1 < \bar{c}_{\text{image}} \cdot \bar{c}_j^+ \leq 2 \\ 0 & \text{else} \end{cases} \quad (5)$$

When segmenting an image, the parameters of the balloon model linearly are interpolated from all parameter sets of the prototypes using the weights  $w_j$ , which depend on the scalar products with the respective adjoint features. The balloon model detects significant contours in the image by a balance of all forces acting on

an edge. Note that mechanical forces strictly are additive. This allows linear interpolation of their strengths.

## 2.4 Color images

For color images, the feature vector is composed by combining the within- and cross-cooccurrence matrices of the color channels [12]. The within-cooccurrence matrices contain separate entries for all color channels using the same displacement whereas the cross-cooccurrence matrices count the presence of image values at the same image position in different channels. For an RGB image, this results in a feature vector containing the cooccurrence matrices of the red, green, and blue channel as well as the cross-cooccurrence between red and green, red and blue, and green and blue. The dimension of this feature vector is six times the dimension of a grayscale feature vector. Since the complexity of similarity measures that are based on adjoint feature vectors only linearly depends on the dimension of the feature vectors, the method can be applied easily to color images.

External influences for the segmentation method are combined from all color channels and weighted according to the intensity of color gradients that occur at the border of objects of interest in the color channels. This gives also need to set appropriate parameters for each color channel separately. This setting is handled by the automated method described in [6].

## 3 Evaluation and Results

Numerical tests are performed to evaluate the stability of the adjoint vector computation, the segmentation of synthetic phantoms, and that of radiographs taken from diagnostic procedures in clinical routine.

### 3.1 Logarithm of cooccurrence matrix entries

So far, it has been postulated that the use of the logarithm increases the numerical stability of distance measures that are computed from the cooccurrence matrices. A test was performed to validate this supposition.

Four color images were extracted from an endoscopic video of vocal folds. Single frames do not contain textures of high contrast [12] and their histograms are compact. The numerical stability of the computation of adjoint feature vectors were assessed by the error measure

$$e = \max_{i,j=1}^n \left( \bar{c}_i \cdot \bar{c}_j^+ - \delta_{ij} \right) \quad (6)$$

It determines the maximal deviation of the scalar products between all feature vectors and all corresponding vectors of prototypes.

In our test, we used single-precision floating point instructions of a Pentium II processor. The matrix inversion was taken from the image analysis tool KhoroS 2 compiled under Linux with a standard GNU compiler. Using normalized cooccurrence matrices for the feature vectors, the error measure  $e$  reached

unacceptable 0.78. It was reduced to 0.006 applying the logarithm to all entries in the cooccurrence matrices prior to normalization.

### 3.2 Evaluation using synthetic images

Gold-standards yielding a valid segmentation usually do not exist in medical imaging. Inter- as well as intra-observer variability hinder the quantification of segmentation quality. In order to give quantitative measures, 81 synthetic images have been created. These images of the size 128x128 pixel contain a centered object described by  $r < r_0 + \Delta r \sin(k\varphi)$  with  $r_0=50$ ,  $\Delta r=10$  and  $k=5$ . Inside and outside are filled with Gaussian-distributed noise of mean  $\mu_{in}$  and  $\mu_{out}$ , respectively, and standard deviation  $\sigma$ . In order to prevent high gradients at the object's border, the gray values linearly are interpolated from inside to outside within a five pixel region (Fig. 4). Parameters for the creation of synthetic images were combined from  $\mu_{in} \in \{130,140,150\}$ ,  $\Delta\mu = \mu_{out} - \mu_{in} \in \{5,10,20\}$  and  $\sigma \in \{2,6,10\}$ . Each combination is based on three different images, giving an amplitude signal-to-noise ration of

$$SNR = 20 \log \frac{\Delta\mu}{\sigma} \quad (7)$$

ranging from -6dB to 20dB. These images were segmented using either a fixed parameter set trained for the image with  $\mu_{in} = 140$ ,  $\mu_{out} = 150$ , and  $\sigma = 6$  (see the third example from the left in Fig. 4) or using an adaptive parameter set resulting from training of 4 or 8 prototype images from this set, respectively. The mean and Hausdorff (maximum) distances were calculated using the vertex positions in a Chamfer distance-transformed image of the original object. Additionally, the overlap measure

$$O = \frac{A \cap B}{A \cup B} \quad (8)$$

was calculated with  $A$  and  $B$  denoting the segmented and the original object, respectively. Segmentations were accepted for  $O > 85\%$ .

Segmentation using the balloon model fails if a fixed parameter set is used (Tab. 1). The contours either collapse or expand over the object towards the image border resulting in large distances and a small overlap measure. Only one third of all

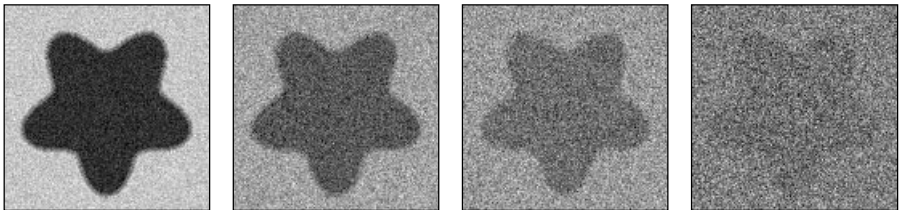


Figure 4: Synthetic images are used for evaluation. The parameters  $(\Delta\mu, \sigma)$  that are used to create the displayed images are from left to right: (20,2), (20,6), (10,6), and (5,10). Note that the images have been histogram optimized for printing.

images is segmented sufficiently without parameter adaptation. Using 4 different images in training, nearly 80% of all segmentations are accepted. The mean difference reduces from about 20 down to 4.4. When 8 different prototypes are trained, the rate of acceptance raises to 89%. Now, the mean distance between all segmentations and the real contour is below 2 pixels. Nevertheless, the average Hausdorff distance about 7 still is notable. In many images, only parts of the contour are detected correctly due to the high amount of noise.

### 3.3 Segmentation of an heterogeneous image archive

The method was applied to a set of 1616 radiographs from the IRMA-project [13]. The images have been taken from daily routine at the Department of Diagnostic Radiology, Medical School, Aachen University of Technology. The radiographs were acquired by several modalities and partly scanned from film using different scanners. Aim of the IRMA-project is content-based access to medical image archives without manual indexing. Therefore, the main contours of imaged body regions have to be segmented automatically without user supervision. First, the balloon model was parameterized by an analysis of the images' histograms. Using the same model, all images were segmented again with the parameters automatically set by the method described above. All together, 19 different appearances have been identified. One of each class was used as a prototype.

All results were manually rated (Fig. 5). A physician either accepted or rejected the segmentation subjectively following his visual impression. Note that it is easier and less time consuming to decide whether a given segmentation result matches the expectation than to draw a manual segmentation. Furthermore, manual reference segmentations are not reproducible.

Using the heuristic histogram analysis, the relevant contours were detected sufficiently in only 496 out of 1616 images. Using the texture adaptation of the balloon model, the automatic segmentation was accepted for 1145 radiographs. The method improves the ratio of acceptance from 31% to 71%. As a main problem, the

parameter set	mean distance $\mu \pm \sigma$	Hausdorff distance $\mu \pm \sigma$	overlap $\mu \pm \sigma$ in %	# accepted / # total
fixed	$19.9 \pm 13,7$	$37.9 \pm 24.7$	$45.1 \pm 38.5$	27 / 81
adaptive, 4 prototypes	$4.4 \pm 7.8$	$9.5 \pm 12.8$	$83.7 \pm 22.7$	64 / 81
adaptive, 8 prototypes	$2.0 \pm 3.6$	$7.1 \pm 10.2$	$90.9 \pm 9.3$	72 / 81

Table 1: Results for the segmentation of synthetic images with and without adaptive parameterization.

segmentation method was disturbed by collimator fields in the radiographs that were neither manually cut nor chosen according to image quality.

## 4. Discussion

Unsupervised segmentation of medical images can be done by balloon models. However, the parameterization of active contours is time consuming and requires expert knowledge on the model so far. Using global texture analysis, this parameterization is done automatically. Numerical robustness of texture calculations is increased by logarithm of cooccurrence matrices that are based on images with similar content and weak texture.

The IRMA archive that is used for evaluation of our method contains images of various regions of body, orientations, imaging modalities and scanning devices. The imaging parameters were not optimized to show contours but for the ability to perform findings in diagnostic regions of interest. Therefore, the increase of 31% to 71% and hence, acceptance of more than two thirds of all segmentations is absolutely reliable. Further improvement may result from optimizing both, texture feature extraction and similarity measures.

So far, the texture-adaptive parameterization method has been used for a balloon model. Note that this method of parameter adjustment is not bound to balloons and could be used for many other segmentation methods that require the choice of appropriate parameters. However, not all segmentation algorithms may be suitable for a linear interpolation of parameters according to the similarity to image prototypes.

## References

1. Duncan JS, Ayache N. Medical Image Analysis: Progress over Two Decades and the Challenges Ahead. *IEEE PAMI* 2000; 22(1): 85-106
2. Mcinerney T, Terzopoulos D. Deformable models in medical image analysis: A survey. *Medical Image Analysis* 1996; 1: 91-108
3. Bredno J, Lehmann T, Spitzer K. A general finite element model for segmentation in 2, 3, and 4 dimensions. *Proc. SPIE* 2000; 3979: 1174-1184
4. Cohen LD, Cohen I. Finite-element methods for active contour models and balloons for 2-D and 3-D images. *IEEE PAMI* 1993; 15(11): 1131-1147

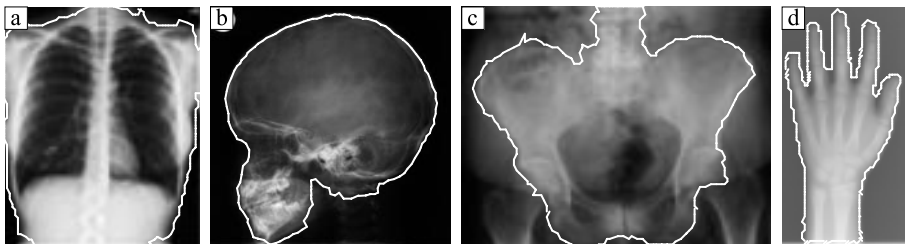


Figure 5: Exemplary segmentations of the categories chest (a), skull (b), pelvis (c), and extremities (d).

5. Kass M, Witkin A, Terzopoulos D. Snakes: Active contour models. *International Journal of Computer Vision* 1988; 1(4): 321-331
6. Bredno J, Lehmann T, Spitzer K: Automatic parameter setting for balloon models. *Proc. SPIE* 2000; 3979: 1185-1208
7. Haralick R, Shanmugam K, Dinstein I. Texture features for image classification. *IEEE SMC* 1973; 3: 610-621
8. Gotlieb C, Kreyzig H. Texture descriptors based on cooccurrence matrices. *Computer Vision, Graphics and Image Processing* 1990; 51: 70-86
9. Walker R, Jackway P, Longstaff I: Recent developments in the use of the co-occurrence matrix for texture recognition. In: *Digital Signal Processing 1997*, 63-65 (Proc. 13th International Conference Santorini, Greece)
10. Lehmann T, Gönner C, Spitzer K. Survey: Interpolation methods in medical image processing. *IEEE MI* 1999; 18(11): 1049-1075
11. Haken H. *Synergetic Computers and Cognition*. Springer Berlin Heidelberg New York, 1991
12. Palm C, Lehmann T, Spitzer K. Color texture analysis of vocal folds using approaches from statistics and signal theory. In: Braunschweig T, Hanson J, Schelhorn-Neise P, Witte H (eds) *Advances in objective laryngoscopy, voice and speech research*. 2000, 49-56 (Proc. 4th International Workshop, Jena, Friedrich-Schiller-University)
13. Lehmann T, Wein B, Dahmen J, Bredno J, Vogelsang F, Kohnen M. Content-based image retrieval in medical applications - a novel multi-step approach. *Proc. SPIE* 2000; 3972: 312-320